Derivation of weakly hydrodynamic models in the Dupuit-Forchheimer regime

Martin Parisot

Highlights

Derivation of weakly hydrodynamic models in the Dupuit-Forchheimer regime

Martin Parisot

- We derive a new hydrodynamic reduced model of the groundwater waves problem within the Dupuit-Forchheimer regime.
- We show that the new model satisfies a energy dissipation law.
- We proposed few simplified models for specific regime, small bedrock variation and weakly non-linear water table.
- We realized a linear analysis of the new models and show the relevance of the new models for intermediate wave numbers.
- We propose entropy-satisfying numerical scheme of the new model and illustrate the differences between the solutions of the models.

Derivation of weakly hydrodynamic models in the Dupuit-Forchheimer regime

Martin Parisot

[a] *Inria, Univ. Bordeaux, CNRS, Bordeaux INP, IMB, UMR 5251, 200 Avenue de la Vieille Tour, Talence, 33405, France*

Abstract

The current study is dedicated to the formal derivation of a hierarchic of asymptotic models that approximate the groundwater waves problem within the Dupuit-Forchheimer regime, over a regular, non-planar substratum. The derivation methodology employed bears resemblance to the techniques utilized in hierarchic of asymptotic models for approximating the water waves problem in the shallow water regime. Mathematically speaking, the asymptotic models manifest as nonlinear, non-local diffusion equations. We identify an energy dissipation law inherent to these models, thereby bolstering the physical validity and confidence in the proposed framework. A numerical strategy is proposed that preserved at the discrete level the energy dissipation.

Keywords: Groundwater waves, Dupuit-Forchheimer regime, Unconfined aquifer, Non-hydrostatic model, Finite volume method, Entropy satisfying scheme

1. Introduction

The current study is dedicated to the formal derivation of a hierarchic of asymptotic models that approximate the groundwater waves problem within the Dupuit-Forchheimer regime, over a regular, non-planar substratum. The groundwater waves problem pertains to the mathematical representation of the phreatic water's evolution, with a specific focus on neglecting the unsaturated vadose zone dynamics over an unconfined aquifer. In recent years, the groundwater waves problem has garnered significant attention from both researchers and practicing engineers. This heightened interest can be attributed to various factors, notably climate change, increasing demands on water resources, pumping activities, and challenges related to saltwater intrusion in

coastal regions. Mathematically, the groundwater waves problem is characterized as a three-dimensional free-surface problem, with flow dynamics governed by Darcy's law. However, for applications on large spatial scales, direct numerical simulations of the groundwater waves problem often become computationally prohibitive. To circumvent these challenges, especially in the context of shallow aquifers, the groundwater waves problem can be effectively simplified through a vertically integrated modeling approach, leading to the Dupuit-Forchheimer model [1]. Despite its utility, the Dupuit-Forchheimer model exhibits limitations, particularly in scenarios where vertical velocities are non-negligible. This inadequacy becomes pronounced in the presence of drainage or injection processes [2, 3]. Additionally, the model's efficacy is compromised when confronted with steep bedrock slopes or boundary conditions mandating a significant slope for the water table.

To address these limitations, enhanced models have been introduced in the literature [4, 5], which are formulated based on Hilbert expansions centered around the Dupuit-Forchheimer regime. While these refined models adeptly capture experimental outcomes for minor fluctuations in the groundwater waves, they exhibit deficiencies when confronted with more abrupt variations. Specifically, in such scenarios, the amplitude of high-frequency components escalates, and the energy of the model increase, see §5. Furthermore, it is pertinent to acknowledge several studies that have delineated analytical solutions, particularly in the context of stationary solutions [6, 7].

The foundation of this study rests upon recognizing the parallels between the groundwater waves problem and the water waves problem [8], as well as between the Dupuit-Forchheimer regime and the shallow water regime. This observation has already been made in [9]. The water waves model pertains to the mathematical representation of the evolution of a free-surface incompressible, irrotational, and inviscid fluid, governed by the Euler equations. This model is instrumental in describing phenomena such as river or coastal flows. In the context of shallow flows, the water waves problem can be effectively streamlined through a vertically integrated modeling approach, leading to the shallow water model [10]. To enhance the fidelity of wave propagation within this regime, a hierarchical series of models has been introduced [11]. In §3, our endeavor focuses on deriving analogous models for the Dupuit-Forchheimer regime. We justify the derived models based on key mathematical properties, namely the mass conservation law, the energy dissipation law, and the decay rate of each model. Mass conservation is a fundamental requirement for applications in water resource management. The energy dissipation law is crucial

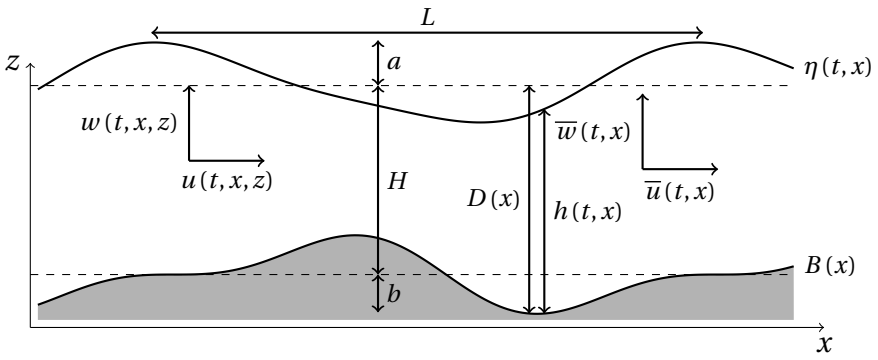

Figure 1: Illustration of model unknowns and characteristic lengths.

for ensuring the long-term stability of a model and serves as a foundational step in analyzing its well-posedness. Moreover, enforcing its discrete counterpart enables the development of robust numerical schemes that validate the accuracy of the approximations. Finally, the decay rate provides a basis for comparing different models and serves as a criterion for selecting the most suitable model depending on the water table dynamics.

Mathematically speaking, the asymptotic models characterizing the Dupuit-Forchheimer regime are classified as nonlinear, non-local diffusion equations [12]. These models bear resemblance to various existing formulations present in the scientific literature. Notable analogues include the Patlak-Keller-Segel equations [13, 14], the Schurtz-Nicolai model [15, 16, 17, 18], the Stokes-Brinkman model [19, 20], and the non-local Exner model [21]. It is imperative to underscore that the computational analysis and numerical solution of these models pose significant challenges, as highlighted in the literature. In §6, we introduce a appropriate numerical strategy to describe the behavior of solutions of the new models. Importantly, this numerical approach ensures the preservation of energy dissipation at the discrete level, as shown in Proposition 5.

2. Hydrodynamic model in porous media

2.1. Governing equations

Consider a flow of an incompressible fluid within a porous medium. Let $S(x,z)$ denote the porosity of the porous medium, defined as the ratio of the volume of voids to the total volume within each elementary volume. Additionally, let $0 \leq s(t,x,z) \leq S(x,z)$ represent the fluid saturation, which is the ratio

of the volume occupied by the fluid to the total volume within each elementary volume. The saturation $s(t,x,z)$ is governed by a conservation law, i.e.

$$\partial_t s + \nabla \cdot (su) + \partial_z (sw) = 0 \tag{1}$$

where $u(t,x,z) \in \mathbb{R}^d$ represents the horizontal fluid velocity, while $w(t,x,z) \in \mathbb{R}$ represents the vertical fluid velocity. We further postulate that the bottom boundary of the porous medium is characterized by a specified elevation function $B(x)$, commonly referred to as the bedrock where a non-penetration condition is enforced i.e.

$$u_{|_{z=B}} \cdot \nabla B - w_{|_{z=B}} = 0. \tag{2}$$

Within the porous medium, the fluid flow is governed by the Darcy's law, which establishes a relationship between the fluid velocity and the pressure field $p(t,x,z)$, i.e.

$$u = -\kappa \nabla p \qquad \text{and} \qquad w = -\kappa \left(\partial_z p + g\right) \tag{3}$$

with $\kappa(x,z) > 0$ represents the permeability of the porous medium, and g denotes the gravitational acceleration. One of the most challenging aspects of modeling fluid flow in porous media lies in accurately describing the pressure field p. In the present work, we focus on dynamics of the groundwater waves. We will see in the next section, under the assumption of predominantly horizontal flow, the pressure field becomes predominantly governed by the dynamics of the water table. This holds true even when considering the effects of weakly hydrodynamic terms.

2.2. Dynamics of the groundwater waves

In this study, our primary focus is directed towards the dynamics of the groundwater waves. We introduce an unknown elevation function, denoted as $\eta(t,x)$, which represents the water table. By definition, the flow under the water table is assumed to be saturated, i.e.

$$s(t,x,z) = \begin{cases} 0 & \text{, if } z > \eta(t,x), \\ S(x,z) & \text{, if } B(x) \le z \le \eta(t,x). \end{cases} \tag{4}$$

The water table satisfies a kinematic equation given by

$$\partial_t \eta + u_{|_{z=\eta}} \cdot \nabla \eta - w_{|_{z=\eta}} = 0. \tag{5}$$

Although it is beyond the scope of the current study, we mention here that considering the media above the water table as partially saturated in water would

involve to add a source term in the kinematic equation. This source term encompasses both the water infiltration rate and the rising water attributed to capillary action. As a consequence of (4), it is deduced that the subsurface flow beneath the water table adheres to a divergence-free condition, expressed as

$$\nabla \cdot (Su) + \partial_z (Sw) = 0. \tag{6}$$

Also the pressure is assumed to be constant at the water table, i.e.e $p\left(t, x, \eta(t,x)\right) = P_a$. Equations (2), (3), (5) and (6) collectively formulate the model design as the groundwater waves problem [22].

Let us first highlight that the groundwater waves problem conserve the volume of water. By vertically integrating (1) from the bedrock to the water table, using Leibniz integral rules, and accounting for the non-penetration condition (2) and the kinematic equation (5), the evolution of the water table is obtained as

$$\partial_t V + \nabla \cdot \left(V \overline{u}\right) = 0 \tag{7}$$

where the water depth reads $h(t,x) = \eta(t,x) - B(x)$, the water volume by unit of surface given by

$$V(x,h) := \int_{B(x)}^{B(x)+h} S(x,z)\, \mathrm{d}z \geq 0$$

and the mean horizontal velocity defined by

$$\overline{u}(t,x) = \frac{1}{V(t,h(t,x))} \int_{B(x)}^{B(x)+h(t,x)} S(x,z)\, u(t,x,z)\, \mathrm{d}z.$$

Alternatively, some may express (7) in its non-conservative form as

$$S_{|_{z=h+B}} \partial_t h + \nabla \cdot \left(\overline{S} h \overline{u}\right) = 0 \tag{8}$$

where $\overline{S}$ denotes the mean porosity, defined as $\overline{S}(x,h) = \frac{V(x,h)}{h} \geq 0$.

Also, we highlight that the groundwater waves problem satisfies an energy dissipation law. Specifically, by defining the energy as

$$\mathscr{E}(x,h) = g \int_{B(x)}^{B(x)+h} S(x,z)\, z\, \mathrm{d}z. \tag{9}$$

To underscore the energy dissipation law, we also introduce the hydrodynamic pressure as the deviation from the hydrostatic pressure, i.e.

$$q(t,x,z) = \frac{1}{\mu}\left(p(t,x,z) - P_a - g\left(\eta(t,x) - z\right)\right)$$

with the shallowness parameter $\mu \in \mathbb{R}$ is taken arbitrarily at this stage. Note that by construction $q\big(t,x,\eta(t,x)\big) = 0$. With this new variable, the Darcy law (3) reads

$$u = -g\overline{\kappa}\nabla(h+B) - \mu\overline{\kappa}\nabla q \qquad \text{and} \qquad w = -\mu\overline{\kappa}\partial_z q. \tag{10}$$

Proposition 1. *Let η be solution of the groundwater waves problem (2), (3), (5) and (6). Then the potential energy (9) satisfies the following dissipation law*

$$\partial_t \mathscr{E} + \nabla\cdot\left(\int_B^{B+h} \big(g(h+B)+\mu q\big) Su\,\mathrm{d}z\right) = -\int_B^{\eta} \frac{S}{\kappa}\left(|u|^2+w^2\right)\mathrm{d}z.$$

Proof. The derivative of the energy with respect to the water depth is given by

$$\partial_h \mathscr{E}(x,h) = g(h+B)\, S_{|_{z=h+B}}.$$

Multiplying (8) by the potential $g(h+B)$, we obtain

$$\begin{aligned} 0 &= g(h+B)\left(S_{|_{z=h+B}}\partial_t h + \nabla\cdot\left(\overline{S}h\overline{u}\right)\right) \\ &= \partial_t \mathscr{E} + \nabla\cdot\left(g(h+B)\,\overline{S}h\overline{u}\right) - g\overline{S}h\overline{u}\cdot\nabla(h+B). \end{aligned} \tag{11}$$

On the other hand, using the Darcy law (10) and the

$$\begin{aligned} \frac{S}{\kappa}\left(|u|^2+w^2\right) = &-gSu\cdot\nabla(h+B) - \nabla\cdot\left(\mu q Su\right) - \partial_z\left(\mu q Sw\right) \\ &+\mu q\left(\nabla\cdot(Su) + \partial_z(Sw)\right). \end{aligned}$$

Using (6), the last term vanishes. By integrating the last equation and using Leibniz integral rule, we get

$$\begin{aligned} \int_B^{B+h} \frac{S}{\kappa}\left(|u|^2+w^2\right)\mathrm{d}z = &-g\overline{S}h\overline{u}\cdot\nabla(h+B) - \nabla\cdot\left(\mu\int_B^{B+h} qSu\,\mathrm{d}z\right) \\ &+\mu q_{|_{z=h+B}} S_{|_{z=h+B}}\left(u_{|_{z=h+B}}\cdot\nabla(B+h) - w_{|_{z=h+B}}\right) \\ &-\mu q_{|_{z=B}} S\left(u_{|_{z=B}}\cdot\nabla(B+h) - w_{|_{z=B}}\right). \end{aligned}$$

The two last terms vanish because the hydrodynamic pressure vanishes at surface $q_{|_{z=h+B}} = 0$ and because of the non-penetration condition (2). Back to (11), we conclude the dissipation law. □

Last but not least, we delve into the analysis of the decay rate of the groundwater wave model. The decay rate characterizes the time it takes for a small disturbance to return to equilibrium as function of its wave number. This analysis

is based on a a linearized version of the model. Moreover, all the parameters, i.e. the permeability, the porosity and the substratum are considered constant, i.e. $\nabla S = \nabla\kappa = \nabla B = 0$ and $\partial_z S = \partial_z \kappa = 0$. This analysis bears resemblance to the dispersion relation analysis employed in water waves problem [23]. Such dispersion relations have proven instrumental in comparing and evaluating the asymptotic shallow water models.

Let us turn our attention to the linearized groundwater waves problem. A curl-free condition emerges as a consequence of Darcy's equation (3), specifically

$$\text{Curl}\left(\frac{1}{\kappa}\begin{pmatrix} u \\ w \end{pmatrix}\right) = 0. \tag{12}$$

From this, we deduce the existence of a potential $\phi(t,x,z)$ such that $u(t,x,z) = \nabla\phi$ and $w(t,x,z) = \partial_z\phi$. The divergence-free condition (6) becomes $\Delta\phi + \partial_z^2\phi = 0$. At the free surface $z = \eta$, the kinematic equation (5) becomes $\partial_t\eta + \nabla\phi \cdot \nabla\eta - \partial_z\phi = 0$. The non-penetration equation over flat substratum (2) becomes $\partial_z\phi = 0$ at $z = -D$. The Darcy's law (3) imply that $\phi = -\kappa\left(p + gz\right)$. Upon linearizing around the state at rest $\left(\eta,\phi\right) = (0,0)$, the linearized groundwater waves problem is

$$\begin{aligned} \Delta\phi + \partial_z^2\phi &= 0\,, \\ \partial_z\phi &= 0\,, \qquad \text{at } z = -D \\ \partial_t\phi + g\overline{\kappa}\partial_z\phi &= 0\,, \qquad \text{at } z = 0. \end{aligned}$$

We seek solutions to the linearized model (2.2), assuming the form $\phi(t,x,z) = \Phi(z)\, e^{ik\cdot x} e^{-\lambda t}$, where k denotes the wave number and λ represents the decay rate. Utilizing the first two equations, we conventionally ascertain that the potential exponentially diminishes with depth. Specifically, the first equation leads to the differential relation $\Phi'' - |k|^2\Phi = 0$. Given the second equation, we deduce that $\Phi(z) = C\cosh(|k|(D+z))$, where C is a constant depending on the initial amplitude perturbation. Subsequently, the third equation results in the relation

$$\widetilde{\lambda}(|kD|) = |kD|\tanh(|kD|) \tag{13}$$

where we introduce the normalized decay rate $\widetilde{\lambda} = \frac{D}{g\overline{\kappa}}\lambda$.

3. Dupuit-Forchheimer regimes

The groundwater waves problem (2), (3), (5), (6) bears notable resemblance to the well-established water waves problem [8]. While a curl-free condition is introduced in the water waves problem, for the groundwater waves problem,

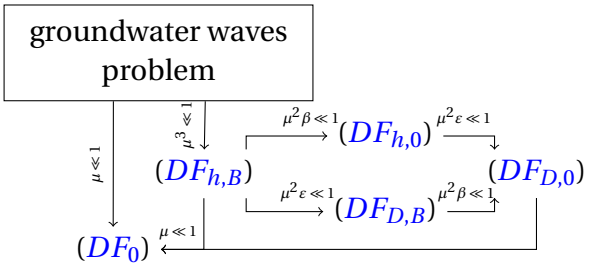

Figure 2: Scheme of the hierarchy of models in the Dupuit-Forchheimer regime.

it emerges as a consequence of Darcy's equation, see (12). The primary distinctions between the groundwater waves problem and the water waves problem lie in the spatial parameters κ and S. Analogous to the water waves problem, the groundwater waves problem poses significant computational challenges due to its three-dimensional nature and the presence of an unknown free-surface boundary. Such intricacy necessitates the derivation of simplified equation sets tailored to specific physical regimes, mimicking the approach adopted for the water waves problem in the shallow water regime. Subsequently, this study proceeds to close the model by approximating the mean horizontal velocity within the Dupuit-Forchheimer regime, wherein the vertical dimension is considerably smaller compared to the horizontal dimension.

We define the fundamental length scales characterizing the flow dynamics. Let H represents the characteristic water depth, L represents the characteristic horizontal length, a represents the mean amplitude of water table fluctuations, and b represents the mean amplitude of bedrock variations, as depicted in Figure 1. The primary dimensional scale for pressure is established by the hydrostatic pressure, expressed as $P = gH$. Leveraging the Darcy's law, it is inferred that the predominant velocity is given by $U = \frac{KgH}{L}$, where K represents the characteristic permeability value, while the characteristic timescale of the flow is defined as $T = \frac{L}{U} = \frac{L^2}{KgH}$. The dimensionless parameters associated with the shallowness of the flow, nonlinearity, and bedrock variations are denoted as $\mu = \frac{H}{L}$, $\epsilon = \frac{a}{H}$, and $\beta = \frac{b}{H}$, respectively. The Dupuit-Forchheimer regime is applicable to shallow flows over sufficiently flat bedrocks, characterized by $\mu \ll 1$. A graphical representation illustrating the hierarchical relationship between the subsequent models is provided in Figure 2.

3.1. The hydrostatic Dupuit-Forchheimer model

Let us start by presenting the well-known asymptotic hydrostatic Dupuit-Forchheimer model [1]. Utilizing the vertical component of Darcy's law (3), it becomes evident that the primary pressure aligns with the hydrostatic pressure, yielding

$$p = g\,(h + B - z) + O\big(\mu\big).$$

Substituting this outcome into the horizontal component of Darcy's law, it can be deduced that the horizontal velocity is dictated by the gradient of the water table

$$u = -g\kappa\nabla\,(h + B) + O\big(\mu\big).$$

This velocity is solely influenced by z through the permeability κ. By vertical integration, we obtain the hydrostatic Dupuit-Forchheimer model defined as

$$\partial_t V - \nabla\cdot\big(g\overline{\kappa}V\nabla(h+B)\big) = 0 \tag{DF_0}$$

with the effective permeability reads $\overline{\kappa}\,(x,h) := \frac{1}{V(x,h)}\int_{B(x)}^{B(x)+h} S\,(x,z)\,\kappa\,(x,z)\,\mathrm{d}z > 0$. This model serves as a $O\big(\mu\big)$-approximation of the groundwater waves model (3), (6), and (7).

We emphasize that the model (DF_0) adheres to an dissipation law of the energy (9).

Proposition 2. *Let h be solution of the hydrostatic Dupuit-Forchheimer model (DF_0). Then the potential energy (9) satisfies the following dissipation law*

$$\partial_t\mathscr{E} - \nabla\cdot\Big(g^2\overline{\kappa}\overline{S}h(h+B)\nabla(h+B)\Big) = -g^2\overline{\kappa}\overline{S}h\,|\nabla(h+B)|^2\,.$$

Proof. Multiplying (DF_0) by the potential $g\,(h+B)$, we obtain

$$\begin{aligned} 0 &= g\,(h+B)\Big(S_{|_{z=h+B}}\partial_t h - \nabla\cdot\Big(g\overline{\kappa}\overline{S}h\nabla\,(h+B)\Big)\Big)\\ &= \partial_t\mathscr{E} - \nabla\cdot\Big(g^2\overline{\kappa}\overline{S}h\,(h+B)\,\nabla\,(h+B)\Big) + g^2\overline{\kappa}\overline{S}h\,|\nabla\,(h+B)|^2 \end{aligned}$$

which confirms the previously stated result. □

After a simple linearization of the hydrostatic Dupuit-Forchheimer model (DF_0), we straightforwardly derive the decay rate as $\widetilde{\lambda}\,(|kD|) = |kD|^2$. The decay rate of the hydrostatic Dupuit-Forchheimer model is a $O\big(\mu\big)$-approximation of the decay rate of the groundwater waves problem (13), confirming the derivation. We plot in Figure 3, the decay rate of the different models for comparison purposes.

3.2. Weakly hydrodynamic fully non-linear model

To enhance the accuracy of the models, we assume that the parameters characterizing the porous media, namely the porosity S and permeability κ, exhibit negligible variations in the vertical direction. Formally, this is expressed as $S(x,z) = \overline{S}(x)$ and $\kappa(x,z) = \overline{\kappa}(x)$. Also considering the flow regular enough, the horizontal velocity can be approximated as constant along the vertical direction, up to a perturbation of order $O(\mu)$. Formally:

$$u(t,x,z) = \overline{u}(x) + O(\mu).$$

Utilizing the divergence-free condition (6), we infer that the vertical velocity predominantly varies linearly with respect to the vertical coordinate. Incorporating the non-penetration condition (2), the vertical velocity reads

$$w(t,x,z) = w_{|_{z=B}} - \mu\frac{z-B}{\overline{S}}\nabla\cdot\left(\overline{S}\overline{u}\right) + O(\mu^2) = \mu\left(\beta\overline{u}\cdot\nabla B - \frac{z-B}{\overline{S}}\nabla\cdot\left(\overline{S}\overline{u}\right)\right) + O(\mu^2)$$

which can be decomposed into its vertically averaged and deviation components, $w(t,x,z) = \overline{w}(t,x) + \frac{z-B-\frac{h}{2}}{h}\widetilde{w}(t,x) + O(\mu^2)$ where

$$\overline{w} = \mu\left(\beta\overline{u}\cdot\nabla B - \frac{h}{2\overline{S}}\nabla\cdot\left(\overline{S}\overline{u}\right)\right) \qquad \text{and} \qquad \widetilde{w} = -\mu\frac{h}{\overline{S}}\nabla\cdot\left(\overline{S}\overline{u}\right). \tag{14}$$

With the vertical velocity from (10), we deduce that the hydrodynamic pressure exhibits primarily quadratic behavior with respect to the vertical coordinate

$$q(t,x,z) = \frac{B+h-z}{h}q_B + 3\frac{(z-B)(B+h-z)}{h^2}\left(2\overline{q} - q_B\right) + O(\mu^2)$$

where $\overline{q}(t,x) = \frac{1}{h(t,x)}\int_{B(x)}^{\eta(t,x)} q(t,x,z)\,dz$ represents the mean hydrodynamic pressure, and the hydrodynamic pressure at the bedrock is denoted as $q_B(t,x) = q(t,x,B(x))$. A vertical integration and differentiation with respect to the vertical axis of the vertical velocity in (10) yield

$$h\overline{w} = \overline{\kappa}q_B \qquad \text{and} \qquad h\widetilde{w} = 6\overline{\kappa}\left(2\overline{q} - q_B\right). \tag{15}$$

Using (14), we can express the hydrodynamic pressure as

$$\begin{aligned} q_B &= \mu\left(\beta\frac{h}{\overline{\kappa}}\overline{u}\cdot\nabla B - \frac{h^2}{2\overline{\kappa}\overline{S}}\nabla\cdot\left(\overline{S}\overline{u}\right)\right) \\ \text{and} \quad \overline{q} &= \mu\left(\beta\frac{h}{2\overline{\kappa}}\overline{u}\cdot\nabla B - \frac{h^2}{3\overline{\kappa}\overline{S}}\nabla\cdot\left(\overline{S}\overline{u}\right)\right) + O(\mu^2). \end{aligned} \tag{16}$$

By performing a vertical integration and applying the Leibniz integral rule, the mean horizontal velocity equation reads

$$h\overline{u} = -g\overline{\kappa}h\nabla(h+B) - \mu\overline{\kappa}\left(\nabla\left(h\overline{q}\right) + \beta q_B \nabla B\right). \tag{17}$$

Substituting (16) into (17), we obtain the weakly hydrodynamic fully non-linear Dupuit-Forchheimer model defined as

$$\partial_t V - \nabla\cdot\left(\overline{S}h\left(1+\mu^2\mathscr{T}_{h,B}\right)^{-1}\left(g\overline{\kappa}\nabla(h+B)\right)\right) = 0 \tag{$DF_{h,B}$}$$

where the operator $\mathscr{T}_{h,B}(U)$ is defined as

$$\mathscr{T}_{\mathbf{h},\mathbf{b}}(U) = \alpha_{\mathbf{b}}U + \frac{\overline{\kappa}}{\mathbf{h}}\nabla\left(\frac{\gamma_{\mathbf{h},\mathbf{b}}}{\overline{\kappa}}\cdot U\right) - \frac{\gamma_{\mathbf{h},\mathbf{b}}}{\overline{S}\mathbf{h}}\nabla\cdot\left(\overline{S}U\right) - \frac{\overline{\kappa}}{\mathbf{h}}\nabla\left(\frac{\omega_{\mathbf{h}}}{\overline{\kappa}\overline{S}}\nabla\cdot\left(\overline{S}U\right)\right) \tag{18}$$

$$\text{with}\quad \alpha_{\mathbf{b}} = \beta^2\nabla\mathbf{b}\otimes\nabla\mathbf{b}\,,\quad \gamma_{\mathbf{h},\mathbf{b}} = \beta\frac{\mathbf{h}^2}{2}\nabla\mathbf{b}\quad\text{and}\quad \omega_{\mathbf{h}} = \frac{\mathbf{h}^3}{3}.$$

This model serves as a $O\left(\mu^3\right)$-approximation of the groundwater waves model (3), (6), and (7).

We emphasize that the model ($DF_{h,B}$) adheres to an dissipation law of the energy (9).

Proposition 3. *Let h be solution of the weakly hydrodynamic fully non-linear Dupuit-Forchheimer model ($DF_{h,B}$). Then the potential energy (9) satisfies the following dissipation law*

$$\partial_t\mathscr{E} + \nabla\cdot\left(\left(g(h+B)+\mu\overline{q}\right)\overline{S}h\overline{u}\right) = -\frac{\overline{S}h}{\overline{\kappa}}\left(\left|\overline{u}\right|^2 + \overline{w}^2 + \frac{\widetilde{w}^2}{12}\right)$$

where the horizontal velocity, the vertical velocities and the hydrodynamic pressures are reconstructed from the water depth as $\overline{u}(x,h) = -g\left(1+\mu^2\mathscr{T}_{h,B}\right)^{-1}\left(\overline{\kappa}\nabla(h+B)\right)$, (14) and (15) respectively.

Proof. Multiplying ($DF_{h,B}$) by the potential $g(h+B)$, we obtain

$$\partial_t\mathscr{E} + \nabla\cdot\left(g(h+B)\overline{S}h\overline{u}\right) = g\overline{S}h\overline{u}\cdot\nabla(h+B).$$

The right-hand side can be estimated by multiplying (17) by $\overline{u}$

$$g\overline{S}h\overline{u}\cdot\nabla(h+B) = -\frac{\overline{S}h\left|\overline{u}\right|^2}{\overline{\kappa}} - \mu\nabla\cdot\left(\overline{q}\overline{S}h\overline{u}\right) + \mu h\overline{q}\nabla\cdot\left(\overline{S}\overline{u}\right) - \mu\beta q_B\overline{S}\nabla B\cdot\overline{u}.$$

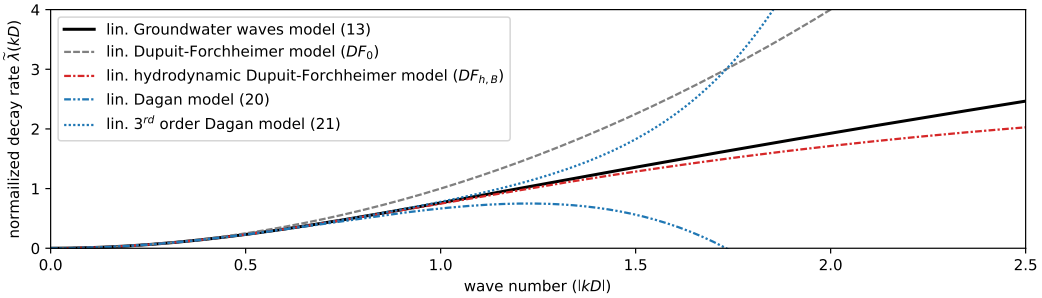

Figure 3: Decay rates corresponding to the linearized groundwater waves problem (13), to the hydrostatic model (DF_0), to the linearized second order Dagan model (20), to the linearized third order Dagan model (21) and to the linearized hydrodynamic model ($DF_{h,B}$).

Similarly, by multiplying the two equations of (15) respectively by $\overline{w}$ and $\widetilde{w}$, we obtain

$$\frac{\overline{S}h\overline{w}^2}{\overline{\kappa}} = q_B\overline{S}\overline{w} \qquad \text{and} \qquad \frac{\overline{S}h\widetilde{w}^2}{\overline{\kappa}} = 6\overline{S}\left(2\overline{q}-q_B\right)\widetilde{w}.$$

Summing up the last three relations, we obtain

$$\begin{aligned} g\overline{S}h\overline{u}\cdot\nabla\left(h+B\right) = &-\frac{\overline{S}h}{\overline{\kappa}}\left(\left|\overline{u}\right|^2+\overline{w}^2+\frac{\widetilde{w}^2}{12}\right)-\mu\nabla\cdot\left(\overline{S}h\overline{q}\overline{u}\right)\\ &+\overline{q}\left(\mu h\nabla\cdot\left(\overline{S}\overline{u}\right)+\overline{S}\widetilde{w}\right)-q_B\overline{S}\left(\mu\beta\nabla B\cdot\overline{u}-\overline{w}+\frac{\widetilde{w}}{2}\right). \end{aligned}$$

Given that the last two terms vanish due to (14), we can conclude the result. □

Remark 1. *The current study mainly concentrates on unbounded domains. However, it's noteworthy to observe that the natural boundary conditions of the hydrodynamic models are established on $\overline{u}$ (or $h\overline{u}$) rather than the water depth h. Physically, this corresponds to imposing the flux at the boundary. Simulating a fixed water depth at the boundary appears to be more intricate and is beyond the scope of this study.*

After a simple linearization of the hydrodynamic Dupuit-Forchheimer model ($DF_{h,B}$), we straightforwardly derive the decay rate as $\widetilde{\lambda}\left(|kD|\right) = \frac{|kD|^2}{1+\frac{1}{3}|kD|^2}$. The decay rate of the hydrodynamic Dupuit-Forchheimer model is a $O\left(\mu^2\right)$-approximation of the decay rate of the groundwater waves problem (13), confirming the derivation.

In Figure 3, the decay rates of each model are depicted. A significant difference in decay rates is observed at high frequencies among the models. Specifically, while high frequencies are damped extremely rapidly in the linearized hydrostatic model (DF_0). Conversely, the high frequencies in the solution of the linearized hydrodynamic model ($DF_{h,B}$) are damped at a bounded rate. This observation suggests that the linearized hydrodynamic model described by equation ($DF_{h,B}$) does not regularize the solution for discontinuous initial conditions, unlike the hydrostatic model (DF_0). The decay rates of the linearized Dagan model (20) (see [4]) and the third order Dagan model (see §5) are also depicted for comparison purposes. These results are described in the corresponding section.

4. Simplified weakly hydrodynamic models

This section focuses on simplified versions of ($DF_{h,B}$), applicable when the model is weakly nonlinear or when bedrock variations are small. Notably, these simplified models retain the same decay rate as the original model ($DF_{h,B}$), since the decay rate is derived under the assumptions of a flat bedrock and linearization.

4.1. Fully non-linear small bedrock variation $\varepsilon = O(1)$ and $\beta = O(\mu)$

In scenarios where the variations in bedrock are small, i.e. $\beta \ll 1$, the model ($DF_{h,B}$) can be substantially simplified. Specifically, neglecting the terms in order of β, the weakly hydrodynamic fully non-linear Dupuit-Forchheimer model with small bedrock variations is expressed as

$$\partial_t V - \nabla \cdot \left(\overline{S} h \left(1 + \mu^2 \mathcal{T}_{h,0} \right)^{-1} \left(g \overline{\kappa} \nabla \left(h + B \right) \right) \right) = 0 \qquad (DF_{h,0})$$

where the operator $\mathcal{T}_{\mathbf{h},0}(U)$ is defined as (18) simply reads

$$\mathcal{T}_{\mathbf{h},0}(U) = -\frac{\overline{\kappa}}{\mathbf{h}} \nabla \left(\frac{\omega_{\mathbf{h}}}{\overline{\kappa}\,\overline{S}} \nabla \cdot \left(\overline{S} U \right) \right). \qquad (19)$$

This model serves as a $O(\mu^2\beta, \mu^3)$-approximation of the groundwater waves model (3), (6), and (7).

We emphasize that the model ($DF_{h,0}$) adheres to an energy dissipation law.

Proposition 4. *Let h be solution of the weakly hydrodynamic fully non-linear model Dupuit-Forchheimer model with small bedrock variations ($DF_{h,0}$). Then the potential energy (9) satisfies the following dissipation law*

$$\partial_t \mathscr{E} + \nabla \cdot \left(\left(g\left(h+B\right) + \mu \overline{q} \right) \overline{S} h \overline{u} \right) = -\frac{\overline{S}h}{\overline{\kappa}} \left(\left| \overline{u} \right|^2 + \frac{\widehat{w}^2}{3} \right)$$

where the horizontal velocity, the vertical velocities and the hydrodynamic pressures are reconstructed from the water depth as $\overline{u}\left(x,h\right) = -g\left(1+\mu^2 \mathscr{T}_{h,B}\right)^{-1}\left(\overline{\kappa}\nabla\left(h+B\right)\right)$, $\widehat{w} = -\mu \frac{h}{\overline{S}} \nabla \cdot \left(\overline{S}\overline{u} \right)$ *and* $\overline{q} = \frac{h}{3\overline{\kappa}} \widehat{w}$.

Proof. The proof is similar to the proof of Proposition 3. □

4.2. Weakly non-linear large bedrock variation $\varepsilon = O\left(\mu\right)$ and $\beta = O\left(1\right)$

In scenarios where the variations in water table are small, i.e. $\varepsilon \ll 1$, the model ($DF_{h,B}$) can be substantially simplified. Specifically, the water depth can be advantageously replaced by the mean depth defined as $D\left(x\right) = H + B\left(x\right) - \int_\Omega B\left(x\right) \mathrm{d}x$, see Figure 1, the weakly hydrodynamic weakly non-linear Dupuit-Forchheimer model is expressed as

$$\partial_t V - \nabla \cdot \left(\overline{S} h \left(1+\mathscr{T}_{D,B}\right)^{-1} \left(g\overline{\kappa}\nabla\left(h+B\right)\right)\right) = 0 \qquad (DF_{D,B})$$

where $\mathscr{T}_{\mathbf{h},\mathbf{b}}$ is defined in (18). This model serves as a $O\left(\mu^2\varepsilon, \mu^3\right)$-approximation of the groundwater waves model (3), (6), and (7).

The advantage of the weakly non-linear model ($DF_{D,B}$) is that the operator $\mathscr{T}_{D,B}$ remains independent of time, in contrast to the operator $\mathscr{T}_{h,B}$ in the model ($DF_{h,B}$). Indeed, the weakly non-linear model ($DF_{D,B}$) come with two significant limitations, which have been previously discussed in the context of reduced models for water waves problem. Firstly, the energy dissipation properties observed in fully non-linear models, as described by Proposition 3 and Proposition 4, do not hold true for weakly non-linear models. Secondly, weakly non-linear models encounter issues at dry fronts, where the mean depth $D(x)$ approaches zero.

4.3. Weakly non-linear small bedrock variation $\varepsilon = O\left(\mu\right)$ and $\beta = O\left(\mu\right)$

In scenarios where both the variations in water table and the variations of bedrock are small, i.e. $\varepsilon \ll 1$ and $\beta \ll 1$, both simplifications can be carried out simultaneously. The weakly non-linear model on small bedrock defined as

$$\partial_t V - \nabla \cdot \left(\overline{S} h \left(1+\mathscr{T}_{D,0}\right)^{-1} \left(g\overline{\kappa}\nabla\left(h+B\right)\right)\right) = 0 \qquad (DF_{D,0})$$

where $\mathscr{T}_{\mathbf{h},0}$ is defined in (19). This model serves as a $O\left(\mu^2\varepsilon, \mu^2\beta, \mu^3\right)$-approximation of the groundwater waves model (3), (6), and (7).

5. Approximation of the non-local operator by Taylor expansion

It is noteworthy that the inverses of the operators $\mathscr{T}_{h,B}(U)$ and $\mathscr{T}_{h,0}(U)$ can be approximated for small μ using Taylor expansion techniques, maintaining consistent modeling precision. Specifically, for the simplest weakly hydrodynamic fully non-linear Dupuit-Forchheimer model on small bedrock ($DF_{h,0}$), the inverse can be expressed as

$$\begin{aligned}\left(1+\mu^2\mathscr{T}_{h,0}\right)^{-1}(U) = U &+ \mu^2\frac{\overline{\kappa}}{h}\nabla\left(\frac{\omega_h}{\overline{\kappa}\overline{S}}\nabla\cdot\left(\overline{S}U\right)\right)\\ &+\mu^4\frac{\overline{\kappa}}{h}\nabla\left(\frac{\omega_h}{\overline{\kappa}\overline{S}}\nabla\cdot\left(\frac{\overline{\kappa}\overline{S}}{h}\nabla\left(\frac{\omega_h}{\overline{\kappa}\overline{S}}\nabla\cdot\left(\overline{S}U\right)\right)\right)\right)+O\left(\mu^6\right).\end{aligned}$$

Truncated at order of μ^4, this reveals that the model introduced in [4, 9], defined by

$$\partial_t V - \nabla\cdot\left(g\overline{\kappa}\overline{S}\left(h\nabla(h+B)+\mu^2\nabla\left(\frac{\omega_h}{\overline{\kappa}\overline{S}}\nabla\cdot\left(\overline{\kappa}\overline{S}\nabla(h+B)\right)\right)\right)\right)=0. \tag{20}$$

This model serves as a $O\left(\mu^2\beta, \mu^3\right)$-approximation of the groundwater waves model (3), (6), and (7). Similarly, conducting the same computation with an arbitrary bedrock yields the model proposed in [5], which serves as a $O\left(\mu^3\right)$-approximation of the groundwater waves model (3), (6), and (7).

By applying a straightforward linearization to the Dagan model (20), we directly obtain the decay rate $\widetilde{\lambda}(|kD|) = |kD|^2 - \frac{|kD|^4}{3}$. This decay rate serves as an $O\left(\mu^2\right)$-approximation of the decay rate for the groundwater waves problem (13). However, for sufficiently large wave numbers, the decay rate becomes negative, see Figure 3. This implies that the amplitude of large wave numbers will be amplified, rendering the linearized Dagan model ill-posed unless specific assumptions are imposed on the initial data. Consistently with this observation, the energy (9) associated with solutions of the Dagan model (20) does not exhibit a decreasing trend. Instead, it follows the balance law

$$\begin{aligned}\partial_t\mathscr{E} - \nabla\cdot\left(g^2\overline{\kappa}\overline{S}\left(h^2\nabla h+\mu^2\left(h\nabla\left(\omega_h\Delta h\right)-\omega_h\Delta h\nabla h\right)\right)\right)\\ = -g^2\overline{\kappa}\overline{S}\left(h|\nabla h|^2-\mu^2\omega_h|\Delta h|^2\right).\end{aligned}$$

For high wave numbers, the right-hand side is positive, implying an increase of the energy of the high wave numbers.

Expanding the non-local operator $\mathcal{T}_{h,B}$ to higher orders, up to μ^6-approximation, may potentially enhance the stability and well-posedness of the model without lost (neither gain) of approximation of the groundwater waves problem. Specifically the third order Dagan model can be defined as

$$\begin{aligned}\partial_t V - \nabla\cdot\left(g\overline{\kappa}\overline{S}\left(h\nabla\left(h+B\right)+\mu^2\nabla\left(\frac{\omega_h}{\overline{\kappa}\overline{S}}\nabla\cdot\left(\overline{S}\overline{\kappa}\nabla\left(h+B\right)\right)\right)\right)\right)\\ -\mu^4\nabla\cdot\left(g\overline{\kappa}\overline{S}\left(\nabla\left(\frac{\omega_h}{\overline{\kappa}\overline{S}}\nabla\cdot\left(\frac{\overline{\kappa}\overline{S}}{h}\nabla\left(\frac{\omega_h}{\overline{\kappa}\overline{S}}\nabla\cdot\left(\overline{S}\overline{\kappa}\nabla\left(h+B\right)\right)\right)\right)\right)\right)\right)=0.\end{aligned} \tag{21}$$

By applying a straightforward linearization to the third-order Dagan model (21), we directly obtain the decay rate $\widetilde{\lambda}\left(|kD|\right)=|kD|^2-\frac{|kD|^4}{3}+\frac{|kD|^6}{9}$. This decay rate provides an $O\left(\mu^2\right)$-approximation of the decay rate for the groundwater waves problem (13). Notably, it remains positive for all wave numbers, see Figure 3. As a result, the model is expected to be well-posed, even though it does not satisfy an energy dissipation law. Nonetheless, the third order Dagan model presents significant computational challenges, as it involves the numerical approximation of exceedingly high derivatives.

6. Numerical resolution

6.1. Numerical schemes and analysis

One of the primary applications of the Dupuit-Forchheimer model lies in estimating groundwater waves elevations for long-term scenarios, spanning periods of a year or even a decade. To carry out such simulations, it is imperative to employ an efficient numerical scheme devoid of time-step restrictions, which elucidates the prevalent adoption of implicit schemes for solving the hydrostatic Dupuit-Forchheimer equation (DF_0). The hydrodynamic Dupuit-Forchheimer models deviate from simple parabolic equations due to the non-local operator $\mathcal{T}_{\mathbf{h},\mathbf{b}}$. In this manuscript, our focus is solely on elementary boundary conditions, particularly the wall boundary condition $\overline{u}_{\partial\Omega}\cdot\mathfrak{n}=0$ where $\mathfrak{n}$ denotes the normal to the computational domain boundary. A thorough investigation dedicated exclusively to boundary conditions for weakly hydrodynamic models seems essential, encompassing both continuous and discrete approaches, to provide an appropriate solution.

Let us narrow our description of the discretization tailored for the weakly dispersive fully non-linear model ($DF_{h,B}$). In our endeavor to devise an entropy satisfying scheme, see Proposition 5, we opt not to discretize the scalar

form ($DF_{h,B}$) directly but rather its extended form encompassing (7), (10), (14), and (15). Moreover, to ensure robust performance in scenarios where hydrodynamic terms are negligible, our objective is to recover a conventional 3-points scheme as the parameter μ tends to zero. To achieve this, we introduce a staggered discretization approach.

We consider a tessellation $\mathbb{T}$ of the horizontal domain $\Omega \subset \mathbb{R}^d$, comprising Card $(\mathbb{T})$ star-shaped control volumes. Let $k \in \mathbb{T}$ denote a control volume within the tessellation, $\mathbb{F}_k$ represent the set of its faces, and $\mathfrak{m}_k$ denote its surface area. Furthermore, for a given face f, its length is represented by $\mathfrak{m}_f$, and its neighboring control volume with respect to k is denoted by k_f, i.e. $k \cup k_f = f$. The unit normal pointing outwards from face f to control volume k is denoted by $\mathfrak{n}_k^{k_f}$. The collection of all faces is denoted by $\mathbb{F}$. We introduce the conventional centered discrete differential operators. For a vectorial data discretized at the faces, $V_\star = (V_f)_{f\in\mathbb{F}}$, the divergence on a primal cell $k \in \mathbb{T}$ is defined as

$$\nabla_k^\delta \cdot V_\star = \frac{1}{\mathfrak{m}_k} \sum_{f\in\mathbb{F}_k} V_f \cdot \mathfrak{n}_k^{k_f} \mathfrak{m}_f \tag{22}$$

For scalar data discretized across the cells, $\phi_\star = \left(\phi_k\right)_{k\in\mathbb{T}}$, the gradient in the vicinity of a face $f \in \mathbb{F}$ is defined as

$$\nabla_f^\delta \phi_\star = \frac{\phi_{k_f} - \phi_k}{\delta_f} \mathfrak{n}_k^{k_f}. \tag{23}$$

The characteristic length δ_f depends on the type of meshes employed. For instance, in 1D, $\delta_f = \frac{\mathfrak{m}_k + \mathfrak{m}_{k_f}}{2}$, while for 2D triangles, $\delta_f = \frac{\mathfrak{m}_k + \mathfrak{m}_{k_f}}{\sqrt{3}\mathfrak{m}_f}$. Note that these approximations assume the mesh to be relatively undistorted. For more general meshes, the use of advanced schemes, such as the DDFV discretization, becomes necessary, as discussed in [24, 25]. Furthermore, preserving the kernel of Grad-Div operators at the discrete level poses non-trivial challenges, as highlighted in [26].

We further introduce the following reconstructions. For scalar data discretized at the faces, $\psi_\star = \left(\psi_f\right)_{f\in\mathbb{F}}$, its reconstruction on a primal cell $k \in \mathbb{T}$ is defined as

$$\left[\psi_\star\right]_k = \frac{1}{\mathfrak{m}_k} \sum_{f\in\mathbb{F}_k} \psi_f \frac{\delta_f \mathfrak{m}_f}{2} \tag{24}$$

and for scalar data discretized across the cells, $\phi_\star = \left(\phi_k\right)_{k\in\mathbb{T}}$, its reconstruction

at a face $f \in \mathbb{F}$ is given by

$$[\phi_\star]_f = \frac{\phi_{k_f} + \phi_k}{2}. \tag{25}$$

Lastly, time discretization is achieved using a time step δ_t, such that $t^{n+1} = t^n + \delta_t$.

In this work, we propose a first-order scheme to illustrate the hydrodynamic model ($DF_{h,B}$) and compare it with the hydrostatic model (DF_0). Ensuring the stability of a numerical scheme for ($DF_{h,B}$) is challenging due to the lack of regularization for high wave numbers. To develop a robust scheme, we focus on an entropy-satisfying approach based on the energy dissipation property Proposition 3. The scheme is given by

$$\begin{aligned} \overline{u}_f^{n+1} + \mu^2 \mathcal{T}^f_{h_\star^n, B_\star}\left(\overline{u}_\star^{n+1}\right) &= -g\overline{\kappa}_f \nabla_f^\delta \left(h_\star^{n+1} + B_\star\right) \\ h_k^{n+1} &= h_k^n - \frac{\delta_t}{\overline{S}_k} \nabla_k^\delta \cdot \left(\overline{S}_\star \left[h_\star^n\right]_\star \overline{u}_\star^{n+1}\right) \end{aligned} \tag{$DF^{\mathrm{L}}_{h,B}$}$$

with the following discretization of the hydrodynamic operator (18)

$$\begin{aligned} \mathcal{T}^f_{\mathbf{h}_\star, \mathbf{b}_\star}(V_\star) = {} & \beta^2 \frac{\overline{\kappa}_f}{[\mathbf{h}_\star]_f} \left[\frac{\mathbf{h}_\star}{\overline{\kappa}_\star \overline{S}_\star} \left[\overline{S}_\star V_\star \cdot \nabla_\star^\delta \mathbf{b}_\star \right]_\star \right]_f \nabla_f^\delta \mathbf{b}_\star \\ & + \beta \frac{\overline{\kappa}_f}{[\mathbf{h}_\star]_f} \left(\nabla_f^\delta \left(\frac{|\mathbf{h}_\star|^2}{2\overline{\kappa}_\star \overline{S}_\star} \left[\overline{S}_\star V_\star \cdot \nabla_\star^\delta \mathbf{b}_\star \right]_\star \right) - \left[\frac{|\mathbf{h}_\star|^2}{2\overline{\kappa}_\star \overline{S}_\star} \nabla_\star^\delta \cdot \left(\overline{S}_\star V_\star \right) \right]_f \nabla_f^\delta \mathbf{b}_\star \right) \\ & - \frac{\overline{\kappa}_f}{[\mathbf{h}_\star]_f} \nabla_f^\delta \left(\frac{|\mathbf{h}_\star|^3}{3\overline{\kappa}_\star \overline{S}_\star} \nabla_\star^\delta \cdot \left(\overline{S}_\star V_\star \right) \right). \end{aligned} \tag{26}$$

To solve the numerical scheme ($DF^{\mathrm{L}}_{h,B}$), we first compute the velocity $\overline{u}_f^{n+1}$ implicitly by substituting the water depth h_k^{n+1} using its corresponding scheme. Once $\overline{u}_f^{n+1}$ is determined, the water depth h_k^{n+1} is then computed explicitly. For physical interpretation, it may be useful to compute the vertical velocities and hydrodynamic pressures, even though they are not required for obtaining the solution. The approximations of the vertical velocities $\overline{w}$ and $\widetilde{w}$ on the control volume $k \in \mathbb{T}$ at time t^{n+1} are given from the horizontal velocity as

$$\begin{aligned} \overline{w}_k^{n+1} &= \frac{\mu}{\overline{S}_k} \left(\beta \left[\overline{S}_\star \overline{u}_\star^{n+1} \cdot \nabla_\star^\delta B_\star \right]_k - \frac{h_k^n}{2} \nabla_k^\delta \cdot \left(\overline{S}_\star \overline{u}_\star^{n+1} \right) \right) \\ \text{and} \qquad \widetilde{w}_k^{n+1} &= -\frac{\mu}{\overline{S}_k} h_k^n \nabla_k^\delta \cdot \left(\overline{S}_\star \overline{u}_\star^{n+1} \right). \end{aligned} \tag{27}$$

and the hydrodynamic pressures as

$$q_{B,k}^{n+1} = \frac{h_k^n}{\overline{\kappa}_k}\overline{w}_k^{n+1} \qquad \text{and} \qquad \overline{q}_k^{n+1} = \frac{h_k^n}{2\overline{\kappa}_k}\left(\overline{w}_k^{n+1} + \frac{\widetilde{w}_k^{n+1}}{6}\right). \tag{28}$$

As it is defined, the scheme is entropy-satisfying, i.e. it ensure the following energy dissipation law.

Proposition 5. *Let h_k^n be the solution of the numerical scheme ($DF_{h,B}^{\mathrm{L}}$). Then the discrete potential energy $\mathscr{E}_k(h) = g\overline{S}_k h\left(\frac{h}{2} + B_k\right)$ adheres to the following dissipation law*

$$\begin{aligned}\mathscr{E}_k\left(h_k^{n+1}\right) + \delta_t \nabla_k \cdot \left(\mathscr{G}_\star^{n+1} + \mathscr{H}_\star^{n+1}\right) \leq \mathscr{E}_k\left(h_k^n\right) \\ - \delta_t\left(\left[\frac{\overline{S}_\star\left[h_\star^n\right]_\star}{\overline{\kappa}_\star}\left|\overline{u}_\star^{n+1}\right|^2\right]_k + \frac{\overline{S}_k h_k^n}{\overline{\kappa}_k}\left(\left|\overline{w}_k^{n+1}\right|^2 + \frac{\left|\widetilde{w}_k^{n+1}\right|^2}{12}\right)\right)\end{aligned}$$

where the numerical energy flux is given by

$$\mathscr{G}_f^{n+1} = \left(g\left[h_\star^n\right]_f\left[h_\star^{n+1} + B_\star\right]_f + \mu\left[h_\star^n \overline{q}_\star^{n+1}\right]_f\right)\overline{S}_f\overline{u}_f^{n+1}$$

and the error in the numerical flux is

$$\mathscr{H}_f^{n+1} = \mu\beta\frac{\delta_f^2}{4}\overline{S}_f\overline{u}_f^{n+1}\cdot\nabla_f^\delta B_\star \nabla_f^\delta q_{B,\star}^{n+1}.$$

The proof is given in Appendix A.

It is worth noting that the scheme ($DF_{h,B}^{\mathrm{L}}$) tends to the classical scheme of the hydrostatic Dupuit-Forchheimer model

$$h_k^{n+1} - \frac{g\delta_t}{\overline{S}_k}\nabla_k^\delta \cdot \left(\overline{\kappa}_\star \overline{S}_\star\left[h_\star^n\right]_\star \nabla_\star^\delta\left(h_\star^{n+1} + B_\star\right)\right) = h_k^n \tag{DF_0^{L}}$$

when the shallowness parameters μ vanishes.

6.2. Numerical results

To illustrate the solutions of the hydrodynamic models, we propose the following test case. We consider a one-dimensional computational domain $\Omega =$

$[0,10]$ with a homogeneous mesh $\mathcal{T} = [1,N] \cap \mathbb{N}$ and a spatial step $\delta_x = \frac{10}{N}$. The substratum is defined by

$$B(x) = -1 + \beta \cos\left(\frac{7\pi x}{10}\right).$$

We impose wall boundaries condition by setting $\overline{u}(t,0) = \overline{u}(t,10) = 0$. The initial condition is given by

$$h^0(x) = 1 + \frac{\varepsilon}{2}\tanh\left(-50\mu(x-5)\right).$$

The parameters β, ε and μ are further defined to analyze the sensitivity of the solution to these parameters.

6.2.1. Sensitivity analysis of numerical parameters

Let's start our analysis by examining the behavior of the numerical scheme under the simplest conditions, characterized by a flat bedrock with parameters $\beta = 0$, $\varepsilon = 1$, and $\mu = 10^{-1}$. In Figure 4, we present the outcomes of the scheme ($DF^{\mathrm{L}}_{h,B}$) with a spatial discretization $\delta_x = 10^{-3}$ and varying time steps δ_t at three distinct times. For comparative purposes, both the initial condition and the solution computed with the hydrostatic model (DF^{L}_0) with $\delta_t = \delta_x$ are included.

A primary observation is the emergence of instabilities for large time steps, specifically when $\delta_t \geq 10^{-4}$. Importantly, these instabilities do not refute the findings of Proposition 5, which asserts the unconditional stability of the solution in the L^2-norm. The temporal evolution of the normalized energy $\frac{\mathscr{E}(t)}{\mathscr{E}(0)}$ is depicted in Figure 5. Consistent with Proposition 5, the energy is decreasing. Notably, at certain points in time, later for smaller time steps, the rate of energy decay decreases, leading to the emergence of instabilities. The origins of these instabilities remain unclear. To mitigate their occurrence, it would be beneficial to investigate stability within the context of Total Variation Diminishing (TVD) norms. However, this exploration presents challenges at both the discrete and continuous levels. Further insights from Figure 5 reveal that the energy decay rate is more gradual for the hydrodynamic model during the initial period. Moreover, Figure 4 highlights that pronounced gradients persist for extended durations as suggest by the linear analysis Figure 3. Nevertheless, over extended time intervals, the hydrodynamic solution eventually converges towards the hydrostatic solution.

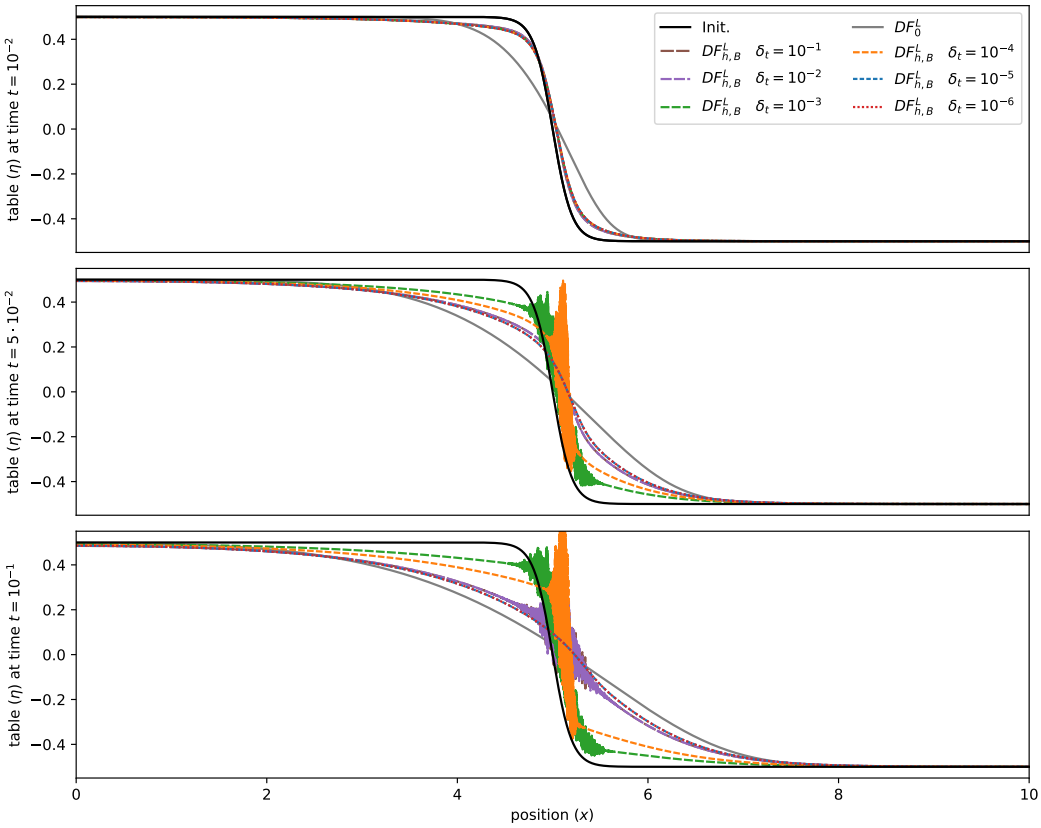

Figure 4: §6.2.1 – Water table elevations computed with $\delta_x = 10^{-3}$ using the hydrostatic model (DF_0^L) with $\delta_t = 10^{-3}$, the hydrodynamic scheme ($DF_{h,B}^L$), is plotted for varying time steps δ_t at $t = 10^{-2}$ (top line), $t = 5 \cdot 10^{-2}$ (middle line), and $t = 10^{-1}$ (bottom line).

In Figure 6, we present the results obtained from various schemes for different spatial step sizes δ_x. The scheme ($DF_{h,B}^L$) is executed with a time step set at $\delta_t = 10^{-5}$. The hydrostatic schemes (DF_0^L) are executed with $\delta_t = \delta_x$. We observe that the space step does not seem to have a significant impact on the results of the hydrodynamic scheme ($DF_{h,B}^L$), unlike the hydrostatic scheme (DF_0^L), which might seem counterintuitive given the presence of strong gradients. Specifically, the scheme ($DF_{h,B}^L$) with $\delta_x = 10^{-1}$ produces outcomes that align closely with the finer resolution using $\delta_x = 10^{-3}$, unlike the scheme (DF_0^L) at time $t = 10^{-2}$. This difference can be explained by the smaller time step used for the hydrodynamic scheme ($DF_{h,B}^L$), and the fact the the schemes are second order in space but only first order in time.

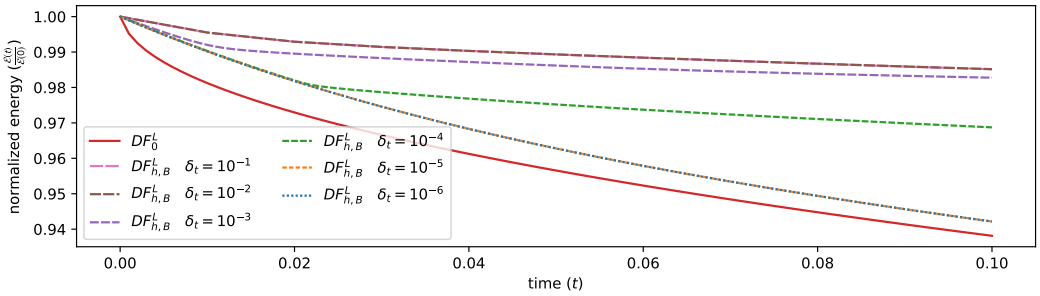

Figure 5: §6.2.1 – Temporal evolution of the normalized energy $\frac{\mathscr{E}(t)}{\mathscr{E}(0)}$, for the scheme ($DF_{h,B}^{\mathrm{L}}$) with $\mu = 10^{-1}$ and $\delta_x = 10^{-3}$, across various time steps δ_t, is depicted. Additionally, the energy profile for the hydrostatic model (DF_0^{L}) with a time step $\delta_t = \delta_x$ is illustrated in red.

6.2.2. *Sensitivity analysis of physical parameters*

We now shift our focus to examining the responses of the various models as the physical parameters undergo variations. For clarity and reduced spurious oscillations, we will exclusively present results with $\delta_x = 10^{-3}$ using the scheme (DF_0^{L}) with $\delta_t = \delta_x$ and the scheme ($DF_{h,B}^{\mathrm{L}}$) with $\delta_t = 10^{-5}$.

On Figure 7, the results of the hydrostatic model (DF_0) and the hydrodynamic model ($DF_{h,B}$) are depicted for $\beta = 0$, $\varepsilon = 1$ and several values of μ. For sufficiently small μ values, the hydrodynamic model ($DF_{h,B}$) closely aligns with the hydrostatic model (DF_0), see bottom line. However, for larger μ values, the hydrodynamic model preserves the pronounced gradient of the water table for a longer duration, a behavior consistent with the linear analysis illustrated in Figure 3. Specifically, for $\mu = 1$, top line of Figure 7, we observe that the initial slope is mainly preserved, even as the amplitude of rapid variations in the water table diminishes. This results in a front that expands into regions with a lower water table level.

On Figure 8, the outcomes of the hydrostatic model (DF_0), the fully non-linear hydrodynamic model ($DF_{h,B}$), and the weakly non-linear hydrodynamic model ($DF_{D,B}$) are presented for $\beta = 0$, $\mu = 10^{-1}$, and various values of ε. The weakly non-linear hydrodynamic model ($DF_{D,B}$) is approximated using the numerical scheme ($DF_{h,B}^{\mathrm{L}}$), with the modification that the hydrodynamic operator $\mathcal{T}^f_{D_\star,B_\star}(V_\star)$, defined in (26), is used in place of $\mathcal{T}^f_{h_\star,B_\star}(V_\star)$. For sufficiently small ε values, the weakly non-linear hydrodynamic model ($DF_{D,B}$) closely aligns

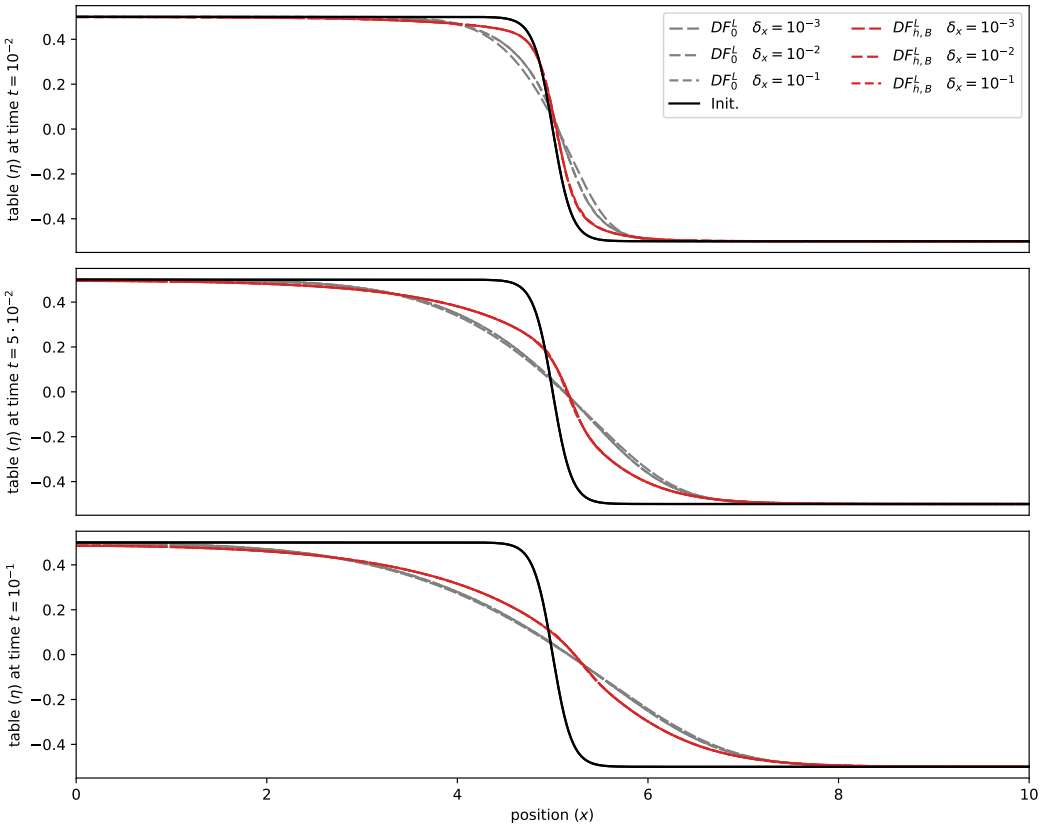

Figure 6: *§6.2.1* – Water table elevations computed using the schemes ($DF_{h,B}^{\mathrm{L}}$) and (DF_0^{L}) across various spatial step sizes at $t = 10^{-2}$ (top line), $t = 5 \cdot 10^{-2}$ (middle line), and $t = 10^{-1}$ (bottom line).

with the fully non-linear hydrodynamic model ($DF_{h,B}$), see bottom line. As ε approaches 1, distinctions between the two models become more noticeable. The divergence between the models becomes particularly pronounced when water depth is minimal (we recall that the substratum is located at $z = -1$), as depicted in the top line of Figure 8. Near dry regions, the solution from the weakly non-linear hydrodynamic model ($DF_{D,B}$) exhibits a steeper profile. Conversely, the fully non-linear hydrodynamic model ($DF_{h,B}$) encounters challenges in defining solutions within dry areas, where $h = 0$. While the weakly non-linear hydrodynamic model ($DF_{D,B}$) provides well-defined solutions in these regions, its applicability might be questionable.

On Figure 9, the results of the models (DF_0), ($DF_{h,B}$), ($DF_{D,B}$), ($DF_{h,0}$), and

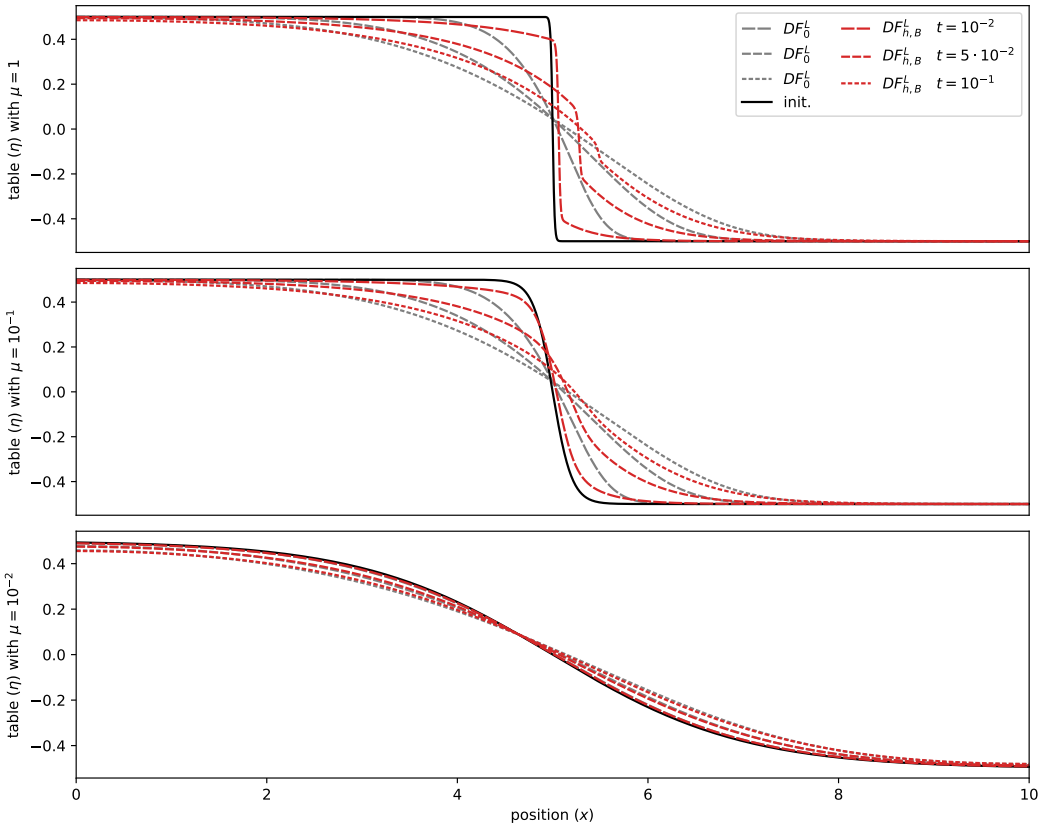

Figure 7: §6.2.2 – Water table elevations computed using the schemes ($DF^{\mathrm{L}}_{h,B}$) and (DF^{L}_{0}) at $t = 10^{-2}$, $t = 5 \cdot 10^{-2}$ and $t = 10^{-1}$ for the parameters $\beta = 0$, $\varepsilon = 1$ and $\mu = 1$ (top line), $\mu = 10^{-1}$ (middle line) and $\mu = 10^{-2}$ (bottom line).

($DF_{D,0}$) are displayed at time $t = 10^{-1}$, with $\mu = 10^{-1}$, $\varepsilon = 1$, and various values of β. The models ($DF_{h,0}$) and ($DF_{D,0}$) are approximated using the numerical scheme ($DF^{\mathrm{L}}_{h,B}$), with the hydrodynamic operators $\mathcal{T}^{f}_{h_\star,0}(V_\star)$ and $\mathcal{T}^{f}_{D_\star,0}(V_\star)$ respectively, as defined in (26), replacing $\mathcal{T}^{f}_{h_\star,B_\star}(V_\star)$. Even for $\beta = 0.1$, distinctions between the solutions obtained from the small bedrock models ($DF_{h,0}$) and ($DF_{D,0}$) and those from the arbitrary bedrock models ($DF_{h,B}$) and ($DF_{D,B}$) are evident. For larger values of β, it is observed that the water table obtained with the small bedrock models ($DF_{h,0}$) and ($DF_{D,0}$) becomes non-monotonic, unlike the water table derived from the arbitrary bedrock models ($DF_{h,B}$) and ($DF_{D,B}$) (refer to $x \in [4,5]$ in the top line of Figure 9). Consistent with prior observations, the water table from the weakly non-linear models ($DF_{D,B}$) and

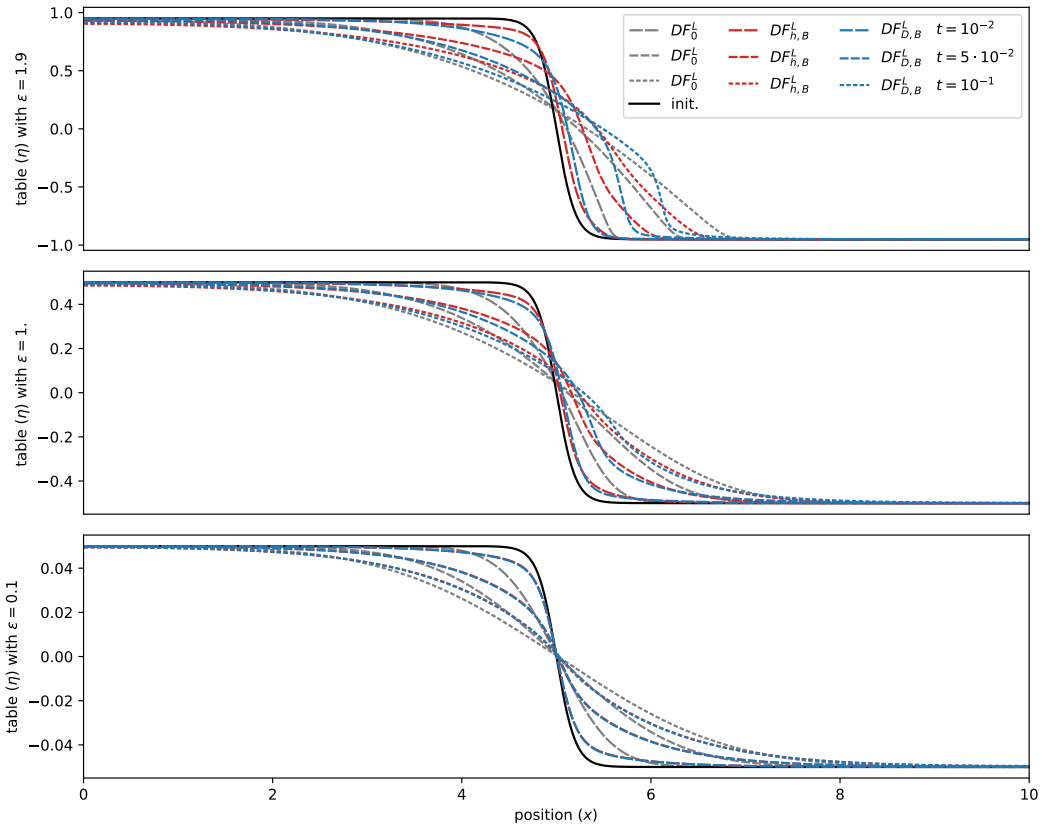

Figure 8: §6.2.2 – Water table elevation obtained with the models (DF_0), ($DF_{h,B}$) and ($DF_{D,B}$) at $t = 10^{-2}$, $t = 5 \cdot 10^{-2}$ and $t = 10^{-1}$ for the parameters $\beta = 0$, $\mu = 10^{-1}$ and $\varepsilon = 1.9$ (top line), $\varepsilon = 1$ (middle line) and $\varepsilon = 10^{-1}$ (bottom line).

($DF_{D,0}$) exhibits steeper gradients when the water depth is minimal. However, in this scenario, it descends below the initial water table level, violating the maximum principle with weakly non-linear models ($DF_{D,B}$) and ($DF_{D,0}$). The maximum principle is well-known for the hydrostatic model (DF_0) but remains unproven for the hydrodynamic model ($DF_{h,B}$). It has been demonstrated for analogous but linear equation see [16]. The applicability of this principle to its discrete counterpart remains an open question. It is worth noting that the numerical simulations never violate the maximum principle with the hydrodynamic model ($DF_{h,B}$).

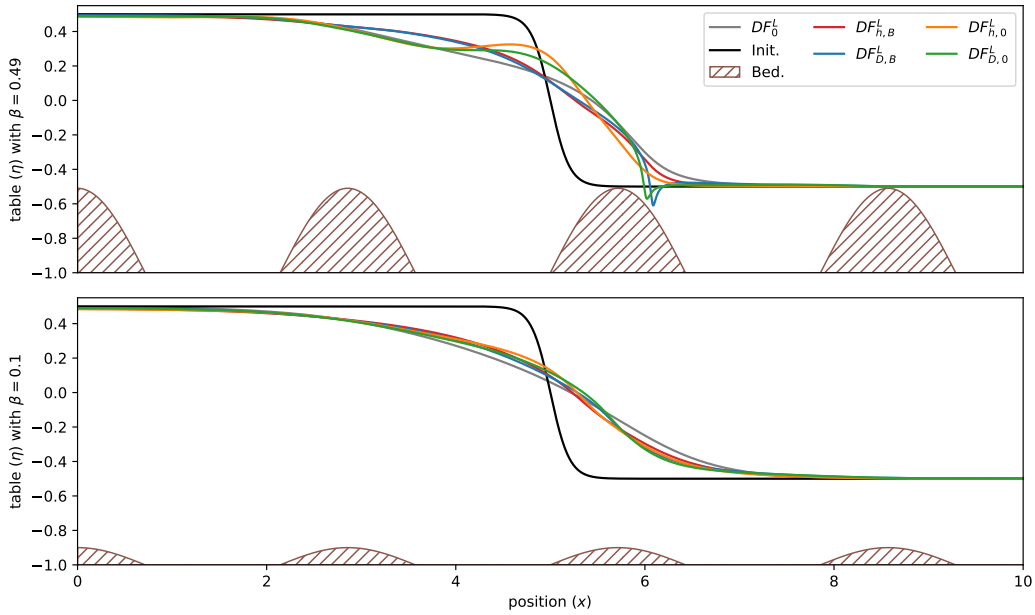

Figure 9: §6.2.2 – Water table elevation obtained with the models (DF_0), ($DF_{h,B}$), ($DF_{D,B}$), ($DF_{h,0}$) and ($DF_{D,0}$) at $t = 10^{-1}$ with $\mu = 10^{-1}$, $\varepsilon = 1$ and $\beta = 0.49$ (top line) and $\beta = 0.1$ (bottom line).

7. Conclusion

In this study, we have developed a hierarchy of reduced models tailored for the groundwater waves problem within the Dupuit-Forchheimer regime, drawing parallels with the shallow water regime in water waves problem. This approach incorporates the first-order effects of hydrodynamic pressure. Our primary model in this hierarchy is both non-linear and non-local in nature. It is designed to accommodate arbitrary variations in both the water table and the bedrock, while also adhering to an energy dissipation law. Furthermore, we have crafted simplified versions of the model to cater to specific scenarios. In the regime characterized by minor variations in bedrock, the non-local operator is notably simplified. In the regime characterized by minor variations in water table, a linearization of the non-local operator can be reasonably used. To provide a comprehensive understanding of the solution behaviors exhibited by these models, we have conducted one-dimensional simulations, offering valuable insights into their performance and applicability.

While our numerical scheme successfully maintains energy dissipation at the discrete level without imposing constraints on the time step, it does ex-

hibit spurious instabilities when subjected to excessively large time steps. The underlying causes of these instabilities remain elusive. A detailed analysis of solution regularity could offer valuable insights to enhance the robustness of our computational approach. Notably, numerical simulations indicate that the fully non-linear model, even when applied over intricate bedrock configurations, consistently preserves solution monotonicity over time. Preserving monotonicity at the discrete level can significantly enhance the robustness of numerical computations. However, it appears that the simplified models within our hierarchy do not maintain this property. Ensuring the robustness of our numerical strategy, particularly when dealing with large time steps, is imperative for applications that encompass expansive space and time scales. Also introducing an a posteriori estimator to facilitate the convergence of the non-linear problem could be a crucial advancement in this direction.

From a mathematical point of view, the derivation technics used in the reduction of water wave models, as presented in [8, 11], seems promising for justifying our groundwater waves reduced models, especially when considering constant permeability and porosity. Another logical progression of this research would involve exploring higher-order hydrodynamic models, akin to those proposed for water waves problem [27, 28, 29]. Natural porous media often consist of horizontal layers with varying compositions and properties. To address this complexity, a layerwise model, following [30], could be explored. Two significant challenges remain in this field that warrant attention. Firstly, boundary conditions, particularly Dirichlet conditions for water depth, need rigorous definition. This would not only validate the model but also facilitate comparisons with analytical solutions and experimental data [6, 7]. Some recent advancements in dispersive free surface models might offer insights that are applicable to our context [31, 32]. Secondly, it's evident that hydrodynamic models are unsuitable in scenarios with discontinuous bottoms, unlike their hydrostatic counterparts. A potential solution could involve space coupling these two models, as previously demonstrated in related studies [17, 33]. Such integrative approaches could potentially overcome this limitation and enhance the applicability of the models in diverse real-world scenarios.

Acknowledgments

This research has been supported by the GeoFun project ANR-19-CE46-0010.

Appendix A. Numerical analysis

Proposition 6. *The discrete operators* (22), (23), (24), *and* (25) *exhibit the following duality property, commonly referred to as the summation-by-part (SBP) property:*

$$\nabla_f \cdot ([\phi_\star]_\star V_\star) = [V_\star \cdot \nabla_\star \phi_\star]_k + \phi_k \nabla_f \cdot V_\star. \tag{A.1}$$

Proof. Upon direct computation, we find

$$\begin{aligned}
\nabla_k^\delta \cdot \left([\phi_\star]_\star V_\star\right) &= \frac{1}{\mathfrak{m}_k} \sum_{f \in \mathbb{F}_k} \frac{\phi_{k_f} + \phi_k}{2} V_f \cdot \mathfrak{n}_k^{k_f} \mathfrak{m}_f \\
&= \frac{1}{\mathfrak{m}_k} \sum_{f \in \mathbb{F}_k} V_f \cdot \frac{\phi_{k_f} - \phi_k}{\delta_f} \mathfrak{n}_k^{k_f} \frac{\delta_f}{2} \mathfrak{m}_f + \frac{\phi_k}{\mathfrak{m}_k} \sum_{f \in \mathbb{F}_k} V_f \cdot \mathfrak{n}_k^{k_f} \mathfrak{m}_f \\
&= \left[V_\star \cdot \nabla^\delta \phi_\star \right]_k + \phi_k \nabla_k^\delta \cdot V_\star.
\end{aligned}$$

□

Proof of Proposition 5. The proof closely follows the proof of Proposition 3. Multiplying the scheme on the water depth, second equation in ($DF^{\mathrm{L}}_{h,B}$) by $g\overline{S}_k \left(h_k^{n+1} + B_k\right)$ and using (A.1), we obtain

$$\begin{aligned}
\mathscr{E}_k^{n+1} \leq \mathscr{E}_k^n &- \delta_t \nabla_k^\delta \cdot (g[h_\star^n]_\star [h_\star^{n+1} + B_\star]_\star \overline{S}_\star \overline{u}_\star^{n+1}) \\
&+ \delta_t g [\overline{S}_\star [h_\star^n]_\star \overline{u}_\star^{n+1} \cdot \nabla^\delta (h_\star^{n+1} + B_\star)]_k.
\end{aligned}$$

Now let us remarque the second equation of ($DF^{\mathrm{L}}_{h,B}$) can be written as

$$\begin{aligned}
[h_\star^n]_f \overline{u}_f^{n+1} = &-g\overline{\kappa}_f [h_\star^n]_f \nabla_f^\delta \left(h_\star^{n+1} + B_\star\right) \\
&-\mu\overline{\kappa}_f \left(\nabla_f^\delta \left(h_\star^n \overline{q}_\star^{n+1}\right) + \beta [q_{B,\star}^{n+1}]_f \nabla_f^\delta B_\star\right)
\end{aligned}$$

with the discrete hydrodynamic pressure defined in (28) and the discrete vertical velocities defined in (27). Multiplying the last equation by $\frac{\overline{S}_f}{\overline{\kappa}_f} \overline{u}_f^{n+1}$, we obtain

$$\begin{aligned}
g\overline{S}_f [h_\star^n]_f \overline{u}_f^{n+1} \cdot \nabla_f^\delta \left(h_\star^{n+1} + B_\star\right) = &-\frac{\overline{S}_f [h_\star^n]_f}{\overline{\kappa}_f} \left|\overline{u}_f^{n+1}\right|^2 \\
&-\mu\overline{S}_f \overline{u}_f^{n+1} \cdot \left(\nabla_f^\delta \left(h_\star^n \overline{q}_\star^{n+1}\right) + \beta [q_{B,\star}^{n+1}]_f \nabla_f^\delta B_\star\right).
\end{aligned}$$

Computing the cell reconstruction of the above equation and using (A.1), we get

$$\begin{aligned} g\left[\overline{S}_\star\left[h_\star^n\right]_\star \overline{u}_\star^{n+1}\cdot\nabla_\star^\delta\left(h_\star^{n+1}+B_\star\right)\right]_k = &-\left[\frac{\overline{S}_\star\left[h_\star^n\right]_\star}{\overline{\kappa}_\star}\left|\overline{u}_\star^{n+1}\right|^2\right]_k \\ &-\mu\nabla_k^\delta\cdot\left(\left[h_\star^n\overline{q}_\star^{n+1}\right]_\star\overline{S}_\star\overline{u}_\star^{n+1}\right)+\mu h_k^n\overline{q}_k^{n+1}\nabla_k^\delta\cdot\left(\overline{S}_\star\overline{u}_\star^{n+1}\right) \\ &-\mu\beta\left[\overline{S}_\star\left[q_{B,\star}^{n+1}\right]_\star\overline{u}_\star^{n+1}\cdot\nabla_\star^\delta B_\star\right]_k. \end{aligned}$$

Focusing on the last term, we write

$$\begin{aligned} &\left[\overline{S}_\star\left[q_{B,\star}^{n+1}\right]_\star\overline{u}_\star^{n+1}\cdot\nabla_\star^\delta B_\star\right]_k \\ &=\frac{1}{\mathfrak{m}_k}\sum_{f\in\mathbb{F}_k}\overline{S}_f\frac{q_{B,k_f}^{n+1}+q_{B,k}^{n+1}}{2}\overline{u}_f^{n+1}\cdot\nabla_f^\delta B_\star\frac{\delta_f\mathfrak{m}_f}{2} \\ &=\frac{q_{B,k}^{n+1}}{\mathfrak{m}_k}\sum_{f\in\mathbb{F}_k}\overline{S}_f\overline{u}_f^{n+1}\cdot\nabla_f^\delta B_\star\frac{\delta_f\mathfrak{m}_f}{2}+\frac{1}{\mathfrak{m}_k}\sum_{f\in\mathbb{F}_k}\overline{S}_f\frac{q_{B,k_f}^{n+1}-q_{B,k}^{n+1}}{\delta_f}\overline{u}_f^{n+1}\cdot\nabla_f^\delta B_\star\frac{\delta_f^2\mathfrak{m}_f}{4} \\ &=q_{B,k}^{n+1}\left[\overline{S}_\star\overline{u}_\star^{n+1}\cdot\nabla_\star^\delta B_\star\right]_k+\nabla_k^\delta\cdot\left(\frac{\delta_\star^2}{4}\overline{S}_\star\overline{u}_\star^{n+1}\cdot\nabla_\star^\delta B_\star\nabla_\star^\delta q_{B,\star}^{n+1}\right) \\ &=q_{B,k}^{n+1}\left[\overline{S}_\star\overline{u}_\star^{n+1}\cdot\nabla_\star^\delta B_\star\right]_k+\frac{1}{\mu\beta}\nabla_k^\delta\cdot\mathscr{H}_\star^{n+1}. \end{aligned}$$

Similarly, multiplying the two equations of (27) by $\frac{\overline{S}_k}{\overline{\kappa}_k}\overline{w}_k^{n+1}$ and $\frac{\overline{S}_k}{\overline{\kappa}_k}\widetilde{w}_k^{n+1}$ respectively, we get

$$\begin{aligned} &\frac{\overline{S}_k h_k^n}{\overline{\kappa}_k}\left|\overline{w}_k^{n+1}\right|^2=\overline{S}_k q_{B,k}^{n+1}\overline{w}_k^{n+1} \\ \text{and}\quad &\frac{\overline{S}_k h_k^n}{\overline{\kappa}_k}\left|\widetilde{w}_k^{n+1}\right|^2=6\overline{S}_k\left(2\overline{q}_k^{n+1}-q_{B,k}^{n+1}\right)\widetilde{w}_k^{n+1}. \end{aligned}$$

Combining all the equations, we conclude that the discrete energy is given by

$$\begin{aligned} &\mathscr{E}_k^{n+1}+\delta_t\nabla_k^\delta\cdot\left(\mathscr{G}_\star^{n+1}+\mathscr{H}_\star^{n+1}\right) \\ &\quad=\mathscr{E}_k^n-\delta_t\left(\left[\frac{\overline{S}_\star\left[h_\star^n\right]_\star}{\overline{\kappa}_\star}\left|\overline{u}_\star^{n+1}\right|^2\right]_k+\frac{\overline{S}_k h_k^n}{\overline{\kappa}_k}\left(\left|\overline{w}_k^{n+1}\right|^2+\frac{\left|\widetilde{w}_k^{n+1}\right|^2}{12}\right)\right) \\ &\qquad+\delta_t\overline{q}_k^{n+1}\left(\mu h_k^n\nabla_k^\delta\cdot\left(\overline{S}_\star\overline{u}_\star^{n+1}\right)+\overline{S}_k\widetilde{w}_k^{n+1}\right) \\ &\qquad+\delta_t q_{B,k}^{n+1}\left(\overline{S}_k\left(\overline{w}_k^{n+1}-\frac{\widetilde{w}_k^{n+1}}{2}\right)-\mu\left[\overline{S}_\star\overline{u}_\star^{n+1}\cdot\nabla_\star^\delta B_\star\right]_k\right). \end{aligned}$$

Using (27), the last two terms cancel out, leading us to conclude. □

References

[1] J. É. J. Dupuit, Études théoriques et pratiques sur le mouvement des eaux dans les canaux découverts et à travers les terrains perméables: avec des considérations relatives au régime des grandes eaux, au débouché à leur donner, et à la marche des alluvions dans les rivières à fond mobile, Dunod, 1863.

[2] H. Bouwer, Limitation of the dupuit-forchheimer assumption in recharge and seepage, Transactions of the ASAE 8 (4) (1965) 512–0515. doi:https://doi.org/10.13031/2013.40565.
URL https://elibrary.asabe.org/abstract.asp?aid=40565&t=3

[3] J. van Schilfgaarde, Limitations of dupuit-forchheimer theory in drainage, Transactions of the ASAE 8 (4) (1965) 515–0516. doi:https://doi.org/10.13031/2013.40566.
URL https://elibrary.asabe.org/abstract.asp?aid=40566&t=3

[4] G. Dagan, Second order linearized theory of free-surface flow in porous media, The Quarterly Journal of Mechanics and Applied Mathematics 20 (4) (1967) 517–526. arXiv:https://academic.oup.com/qjmam/article-pdf/20/4/517/5290698/20-4-517.pdf, doi:10.1093/qjmam/20.4.517.
URL https://doi.org/10.1093/qjmam/20.4.517

[5] Y. Zerihun, Extension of the Dupuit–Forchheimer Model for Non-Hydrostatic Flows in Unconfined Aquifers, Fluids 3 (2) (2018) 42. doi:10.3390/fluids3020042.
URL http://dx.doi.org/10.3390/fluids3020042

[6] O. Castro-Orgaz, J. V. Giráldez, N. I. Robinson, Second-order two-dimensional solution for the drainage of recharge based on picard's iteration technique: A generalized dupuit-forchheimer equation, Water Resources Research 48 (6) (2012). arXiv:https://agupubs.onlinelibrary.wiley.com/doi/pdf/10.1029/2011WR011751, doi:https://doi.org/10.1029/2011WR011751.
URL https://agupubs.onlinelibrary.wiley.com/doi/abs/10.1029/2011WR011751

[7] J. Knight, Improving the dupuit–forchheimer groundwater free surface approximation, Advances in Water Resources 28 (10) (2005) 1048–1056, flow Processes in Hydrology: Contributions of J.-Y. Parlange. doi:https://doi.org/10.1016/j.advwatres.2005.04.014.
URL https://www.sciencedirect.com/science/article/pii/S030917080500134X

[8] D. Lannes, The water waves problem: mathematical analysis and asymptotics, Vol. 188, Mathematical Surveys and Monographs, 2013.

[9] P. Nielsen, R. Aseervatham, J. D. Fenton, P. Perrochet, Groundwater waves in aquifers of intermediate depths, Advances in Water Resources 20 (1) (1997) 37–43. doi:https://doi.org/10.1016/S0309-1708(96)00015-2.
URL https://www.sciencedirect.com/science/article/pii/S0309170896000152

[10] A.-J.-C. B. de Saint-Venant, Théorie du mouvement non permanent des eaux, avec application aux crues des rivières et à l'introduction des marées dans leurs lits, C.R. Acad. Sci. Paris 73 (1871) 147–154.

[11] D. Lannes, P. Bonneton, Derivation of asymptotic two-dimensional time-dependent equations for surface water wave propagation, Physics of Fluids 21 (1) (2009).

[12] C. Bucur, E. Valdinoci, et al., Nonlocal diffusion and applications, Vol. 20, Springer, 2016.

[13] E. F. Keller, L. A. Segel, Traveling bands of chemotactic bacteria: A theoretical analysis, Journal of Theoretical Biology 30 (2) (1971) 235–248. doi:https://doi.org/10.1016/0022-5193(71)90051-8.
URL https://www.sciencedirect.com/science/article/pii/0022519371900518

[14] C. S. Patlak, Random walk with persistence and external bias, The bulletin of mathematical biophysics 15 (3) (1953) 311–338. doi:10.1007/BF02476407.
URL https://link.springer.com/content/pdf/10.1007/BF02476407.pdf

[15] T. Goudon, M. Parisot, Non–local macroscopic models based on gaussian closures for the spizer-härm regime, Kinetic and Related Models 4 (3) (2011) 735–766. doi:10.3934/krm.2011.4.735.
URL http://dx.doi.org/10.3934/krm.2011.4.735

[16] T. Goudon, M. Parisot, On the spitzer–härm regime and nonlocal approximations: Modeling, analysis, and numerical simulations, Multiscale Modeling & Simulation 9 (2) (2011) 568–600. arXiv:https://doi.org/10.1137/100800269, doi:10.1137/100800269.
URL https://doi.org/10.1137/100800269

[17] T. Goudon, M. Parisot, Finite volume schemes on unstructured grids for non-local models: Application to the simulation of heat transport in plasmas, Journal of Computational Physics 231 (24) (2012) 8188 – 8208. doi:https://doi.org/10.1016/j.jcp.2012.07.050.
URL http://www.sciencedirect.com/science/article/pii/S0021999112004548

[18] G. P. Schurtz, P. D. Nicolaï, M. Busquet, A nonlocal electron conduction model for multidimensional radiation hydrodynamics codes, Physics of Plasmas 7 (10) (2000) 4238–4249. doi:10.1063/1.1289512.
URL https://doi.org/10.1063/1.1289512

[19] H. C. Brinkman, A calculation of the viscous force exerted by a flowing fluid on a dense swarm of particles, Flow, Turbulence and Combustion 1 (1) (1949) 27–34. doi:10.1007/BF02120313.
URL https://link.springer.com/content/pdf/10.1007/BF02120313.pdf

[20] M. Krotkiewski, I. S. Ligaarden, K.-A. Lie, D. W. Schmid, On the importance of the stokes-brinkman equations for computing effective permeability in karst reservoirs, Communications in Computational Physics 10 (5) (2011) 1315–1332. doi:10.4208/cicp.290610.020211a.

[21] E. Audusse, L. Boittin, M. Parisot, Asymptotic derivation and simulations of a non-local exner model in large viscosity regime, ESAIM: M2AN 55 (4) (2021) 1635–1668. doi:10.1051/m2an/2021031.
URL https://doi.org/10.1051/m2an/2021031

[22] J. Boussinesq, Recherches théoriques sur l'écoulement des nappes d'eau infiltrées dans le sol et sur le débit des sources, Journal de Mathématiques Pures et Appliquées 5e série, 10 (1904) 5–78.

[23] G. B. Airy, Tides and waves, B. Fellowes, 1845.

[24] K. Domelevo, P. Omnes, A finite volume method for the laplace equation on almost arbitrary two-dimensional grids, ESAIM: Mathematical Modelling and Numerical Analysis 39 (6) (2005) 1203–1249. doi:10.1051/m2an:2005047.
URL http://dx.doi.org/10.1051/m2an:2005047

[25] F. Hermeline, A finite volume method for the approximation of diffusion operators on distorted meshes, Journal of Computational Physics 160 (2) (2000) 481–499. doi:https://doi.org/10.1006/jcph.2000.6466.
URL https://www.sciencedirect.com/science/article/pii/S0021999100964660

[26] D. Arnold, R. Falk, R. Winther, Finite element exterior calculus: from hodge theory to numerical stability, Bulletin of the American mathematical society 47 (2) (2010) 281–354.

[27] B. Khorbatly, I. Zaiter, S. Isrwai, Derivation and well-posedness of the extended green-naghdi equations for flat bottoms with surface tension, Journal of Mathematical Physics 59 (7) (Jul. 2018). doi:10.1063/1.5020601.
URL http://dx.doi.org/10.1063/1.5020601

[28] P. A. Madsen, H. A. Schäffer, Higher–order boussinesq–type equations for surface gravity waves: derivation and analysis, Philosophical Transactions of the Royal Society of London. Series A: Mathematical, Physical and Engineering Sciences 356 (1749) (1998) 3123–3181. doi:10.1098/rsta.1998.0309.
URL https://doi.org/10.1098/rsta.1998.0309

[29] Y. Matsuno, Hamiltonian formulation of the extended Green–Naghdi equations, Physica D: Nonlinear Phenomena 301-302 (2015) 1–7. doi:https://doi.org/10.1016/j.physd.2015.03.001.
URL https://www.sciencedirect.com/science/article/pii/S0167278915000354

[30] E. D. Fernández-Nieto, M. Parisot, Y. Penel, J. Sainte-Marie, A hierarchy of dispersive layer-averaged approximations of Euler equations for free surface flows, Communications in Mathematical Sciences 16 (5) (2018) 1169–1202. doi:10.4310/cms.2018.v16.n5.a1.
URL http://dx.doi.org/10.4310/CMS.2018.v16.n5.a1

[31] D. Lannes, L. Weynans, Generating boundary conditions for a Boussinesq system, Nonlinearity 33 (12) (2020) 6868–6889. doi:10.1088/1361-6544/abaa9e.
URL https://doi.org/10.1088/1361-6544/abaa9e

[32] S. Noelle, M. Parisot, T. Tscherpel, A class of boundary conditions for time-discrete Green-Naghdi equations with bathymetry, SIAM Journal on Numerical Analysis (2022).
URL https://hal.archives-ouvertes.fr/hal-03256700

[33] M. Parisot, Thick interface coupling technique for weakly dispersive models of waves, ESAIM: M2AN 58 (4) (2024) 1497–1522. doi:10.1051/m2an/2024048.
URL https://doi.org/10.1051/m2an/2024048